Atomic Spectroscopy

Article

Self-absorption Coefficient Iteration for Improved Quantitative Analysis in Surface-enhanced Laser-induced Breakdown Spectroscopy

Dongdong Li, Xinyan Yang,* Kelong Liu, Pengfei Huang, Zefeng Hua, Zhengbo Qin, Zhongfa Sun, and Xianfeng Zheng

Anhui Province Key Laboratory for Control and Applications of Optoelectronic Information Materials, Department of Physics, Anhui Normal University, Wuhu 241000, P. R. China

Received: *December 03, 2025;* ***Revised:*** *January 13, 2026;* ***Accepted:*** *January 27, 2026;* ***Available online:*** *January 27, 2026.*

DOI: 10.46770/AS.2025.209

ABSTRACT: Surface-enhanced laser-induced breakdown spectroscopy (SENLIBS), with the advantage of higher detection sensitivity, is widely applied in the field of water quality monitoring. However, the self-absorption effect occurs, which reduces the accuracy of quantitative analysis. To correct for the self-absorption effect, the self-absorption coefficient (SA) iteration method was proposed. This method iteratively calculates the SA through the exponential fitting parameter of standard samples to correct the spectral intensity of standard samples and unknown sample. With this method, the SA values of Cr spectral lines were corrected to be closer to 1. As a result, the average limit of detection (LOD), average of the average relative error (ARE), and average root mean square error of cross-validation (RMSECV) were reduced from 0.118 ppm to 0.057 ppm, 39.94% to 14.00%, and 0.752 ppm to 0.403 ppm, respectively. This demonstrated that SA iteration method could improve the quantitative analysis performance of LIBS by correcting for the self-absorption effect.

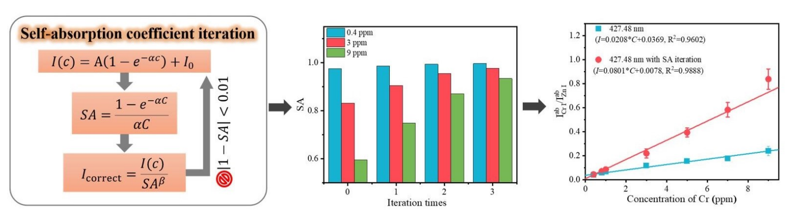

INTRODUCTION

As a cutting-edge spectral enhancement method, surface enhanced laser induced breakdown spectroscopy (SENLIBS) [1] has become a focal point in LIBS-based water quality monitoring [2, 3] due to its distinct advantages, such as the absence of liquid splash, droplet scatter, and surface fluctuation, along with efficient sample preparation, low equipment costs, and heightened sensitivity [4]. In this method, the liquid sample is transformed into a solid layer by dropping it onto a non-absorbent substrate and drying it, which not only increases the enrichment rate of the analytical element but also enhances the plasma emission spectroscopy by ablating both the substrate and the sample layer. Although the sensitivity of LIBS was improved, the nonlinearity of the calibration curve occurred due to the self-absorption effect. Self-absorption effect [5] in LIBS is recognized as one of the predominant factors affecting the accuracy of quantitative analysis[6]. The self-absorption effect can lead to a reduction in spectral line intensity, and in severe cases, may cause a "self-reversal" phenomenon, resulting in concave characteristic spectral line peaks and a decline in the linearity of the calibration curve, thereby diminishing the accuracy of elemental detection. For instance, the use of portable SENLIBS devices for ion analysis in water by Schlatter [7] et al. encountered limitations in direct curve fitting for quantitative analysis due to the spectral saturation effect induced by the self-absorption effect, which ultimately impacts the accuracy of SENLIBS quantitative analysis.

The physical mechanism of the self-absorption effect is inherently linked to spectral line properties and plasma characteristics. In high-density plasmas, self-absorption of elemental spectral lines is particularly pronounced due to substantial optical thickness, which significantly modulates spectral line intensity[8, 9]. To mitigate the self-absorption effect, researchers have optimized experimental parameters such as ambient pressure[10], laser energy[11, 12], acquisition delay[13, 14], and collection position[15, 16] to reduce its impact, but this approach offers limited optimization scope. For further reduction, physical auxiliary techniques have been adopted, such as double pulse[17], telescope methods[18] and laser/microwave-assisted excitation methods[19, 20]. While effective for active self-absorption correction, these strategies increase the complexity and cost of LIBS setups.

Against this backdrop, researchers have developed self-absorption models and correction algorithms to attenuate self-absorption effects[21-25]. For instance, Mansour[23] proposed a self-absorption parameter-based correction method to investigate self-absorption impacts on electron temperature measurements, quantifying and correcting self-absorption in Al atomic lines. Sun *et al*. [24] introduced an internal reference-based self-absorption correction method for calibration-free LIBS (CF-LIBS), which improved the linearity of Boltzmann plots and the accuracy of quantitative results. Aragón[25] *et al.* leveraged the merits of the curve of growth (COG) method to propose an improved Boltzmann plot method, constructed using the COG curve slope at low concentration limits; this eliminated systematic errors in plasma apparent temperature measurements induced by self-absorption. Hou[26] et al. proposed a temperature iterative self-absorption correction method, which continuously calculates and corrects the self-absorption effects using plasma temperature and absorption path length, thereby enhancing the linearity and predictive accuracy of quantitative curves for Cu. For instance, over the sample concentration range of 100–10000 ppm Cu, their method reduced the prediction relative error from 5.71% to 1.42%, improved the R^2 of the calibration curve to 0.998, and enhanced the Boltzmann plot of R^2 from 0.987 to 0.998. Zhang[27] et al. utilized the plasma image reference correction method to determine the SA value, successfully correcting the LIBS quantitative analysis curve linearity (R^2=0.9999). Li[28] et al. proposed the blackbody radiation reference self-absorption correction (BRR-SAC), using blackbody radiation as a reference to correct the self-absorption effect, and through iterative algorithms calculating plasma temperature and optical collection efficiency to achieve self-absorption correction, improving the accuracy of elemental concentration prediction and Boltzmann linearity. Their results, obtained on titanium alloy samples containing Ti 896000–908000 ppm, V 34000–57000 ppm and Al 34000–54000 ppm, showed a reduction in the average relative error to the range of 0.21–0.27%, down from 2.08–3.62%. Rezaei *et al.*[29] verified that after correcting for self-absorption effects, the accuracy of artificial neural networks (ANN) was higher than that of calibration curves, reporting a decrease in the average relative error for Fe from 13.3% to 3.84%. Dong *et al.* [30] used genetic algorithms (GA) to iteratively correct plasma temperatures in CF-LIBS, and the results showed that the CF-LIBS based on GA had higher accuracy in the quantitative analysis of copper alloys than the traditional CF-LIBS method. The samples contained Al 78000–98000 ppm, Fe 30000–49000 ppm, Mn 16000–29000 ppm and Cu 841000–850000 ppm. The new method cut the relative errors of these four elements by more than half and lifted the Boltzmann plot R^2 from below 0.8 to above 0.95. Yang[31] et al. introduced the particle swarm optimization algorithm (PSO) into CF-LIBS analysis, which reduced the self-absorption effects on the analytical lines of various species and enhanced the quantitative analysis capability of CF-LIBS, achieving average relative errors of 4.40%, 6.81%, and 2.29% for Cr 12800–24500 ppm, Ni 17000–19300 ppm, and Fe 545000–193000 ppm concentrations, respectively. While the aforementioned computational correction methods are effective, they typically rely on multi-line analysis, precise atomic parameters, or iterative solutions of plasma state parameters. For instance, the temperature iteration method requires constructing a Boltzmann plot and selecting a set of spectral lines that satisfy local thermodynamic equilibrium conditions, whereas methods based on the curve of growth or physical models demand known or assumed line-broadening parameters and optical thickness models. Consequently, while pursuing high-precision correction, the implementation threshold and computational costs of these methods increase accordingly. For LIBS technology aimed at routine analysis and field monitoring, developing a method that can effectively correct self-absorption while being easy to implement without significantly increasing analytical complexity is a research direction of great practical importance.

To address this, this study proposes a correction method based on self-absorption coefficient iteration. This method utilizes only the intensity-concentration calibration curve shape information of a single analytical line of the target element and directly corrects the spectral intensity for self-absorption through an iterative algorithm. It does not rely on multi-line fitting, complex plasma physical diagnostics (such as temperature measurement), or extensive atomic spectroscopy databases. The fundamental principle is as follows: an empirical nonlinear function is used to fit the saturation trend of the initial calibration curve, from which a self-absorption parameter (α) characterizing the degree of self-absorption is extracted, and the self-absorption coefficient is subsequently calculated. Through iterative refinement of the spectral intensity, this coefficient is driven toward the ideal value of 1, thereby yielding a linearized calibration curve and more accurate quantitative results. This study validates the effectiveness of the method using trace chromium analysis in aqueous solutions via SENLIBS as a model system and compares its performance with that of the traditional temperature iteration method.

EXPERIMENTAL

Sample preparation. The flow chart of the sample preparation procedure is shown in the dashed-line section of Fig. 1. The target

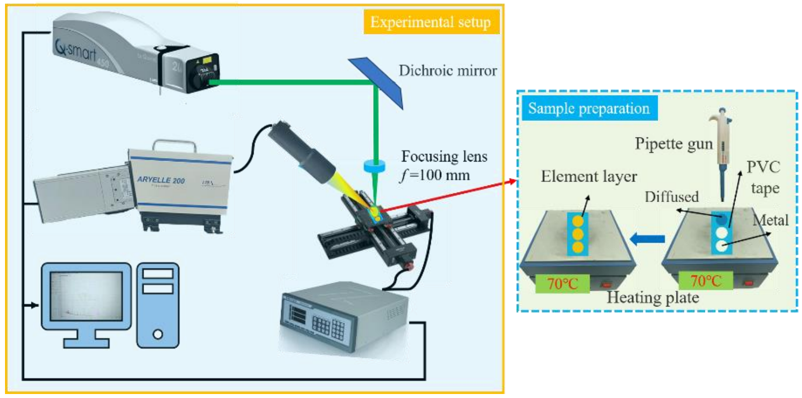

Fig. 1 Schematic diagram of the experimental setup and sample preparation.

analyte was chromium (Cr) element. A stock solution of Cr with a nominal concentration of 20 ppm was prepared by dissolving 10.246 mg of $CrCl_3 \cdot 6H_2O$ crystals (purity 99.999%, Xilong Scientific Co., Ltd, China) in distilled water within a 100 mL volumetric flask. The mass was measured using an electronic balance (precision: 0.1 mg, PTX-FA210, Huazhi Scientific Instrument Co., Ltd., America). Standard solutions were obtained by diluting the stock solution with distilled water. The concentration of Cr in the standard solutions was 0.4, 0.8, 1, 3, 5, 7, and 9 ppm. For SENLIBS sample preparation, commercially pre-polished Zn (99.995%) substrates (1 mm thick) were used as the metal substrate. The elemental analysis report of the zinc substrate confirmed the absence of detectable chromium contamination, with primary impurities being Fe (0.001%), Cd (0.001%), Sn (0.001%), and Cu (0.001%). Before each experiment, they were ultrasonically cleaned with ethanol and distilled water, then air-dried. Each substrate was used only once to prevent cross-contamination and ensure surface consistency. A volume of 400 µL of each standard solution was pipetted into a 16 mm diameter circular hole defined by PVC tape attached to the substrate surface, as detailed in our previous work[32]. Then the standard solution was dried by a thermostatic heating platform (200 mm×200 mm, ANSAI-946C+) with the temperature of 70 °C. The standard solution was formed as a layer on the substrate surface. To validate the reliability of the prepared standard series, the solid SENLIBS samples were independently analyzed using X-ray fluorescence (XRF) spectroscopy. It is important to note that the prepared concentrations of Cr, which is 0.4-9 ppm, correspond to the original aqueous solution. The XRF-tested concentration directly probes the solid residue where Cr was highly enriched on the metal substrate. As shown in Table S1, the XRF-measured concentration exhibits a consistent increasing trend with the prepared solution concentration. This result confirms the successful and consistent preparation of the standard sample series and validates the established concentration gradient, forming the foundation for this methodological study.

Experimental. A single-pulse LIBS experimental setup was used in this experiment as shown in Fig. 1, and its details were described in the previous work[32]. Nd: YAG (Quantel, Q-smart 450) laser, operating at a wavelength of 532 nm with a pulse width of 5 ns and beam diameter of 6 mm, was used to interact with the sample through the dichroic mirror (reflectivity >99.5%) and focusing lens (f=100 mm, Thorlabs). The sample was mounted on a two-dimensional motorized stage (TSA-150) with the speed of 4.5 mm/s to avoid repetitive ablation. The plasma emission was collected by the optics (f=100 mm, Thorlabs) and transmitted via an optical fiber (core diameter: 400 µm, length: 1.5 m) to the Czerny-Turner spectrograph (LTB, ARYELLE 200). The spectrograph, featuring a spectral measurement range of 212-885 nm and a resolution of $\lambda/\Delta\lambda$=8000, was complemented by an ICCD (Andor, iStar DH334T) with a 1024 × 1024 pixel array. Spectral acquisition was controlled using the manufacturer-supplied Sophi software. For higher signal to noise ratio and weaker self-absorption effect, the laser energy, delay time, and gate width was set to 100 mJ, 1.5 µs, and 8 µs, respectively. In this study, the defocus amount is -2.5 mm. The radius of the crater is 157.513 µm by an optical microscope (Nikon, ECLIPSE LV 150N, 5x), and the laser energy density is 128.3 J/cm^2. Each spectral data was accumulated 100 shots, and 10 spectral data of each sample were detected.

Data processing. The raw spectra were processed sequentially before quantitative analysis. First, background correction was applied using a two-point background subtraction method. Then, to compensate for plasma fluctuations, the intensity of each Cr line was normalized to the Zn I 468.01 nm line from the Zn substrate, serving as an internal standard, according to the equation: $I_{normalized} = I_{Cr} / I_{Zn}$.

The core iterative self-absorption correction algorithm, as detailed in the Methodology subsection and illustrated in Fig. 2, was then applied. All data processing steps, including background correction, normalization, the execution of the iterative algorithm, and figure generation, were implemented using Origin (Version 2021) software.

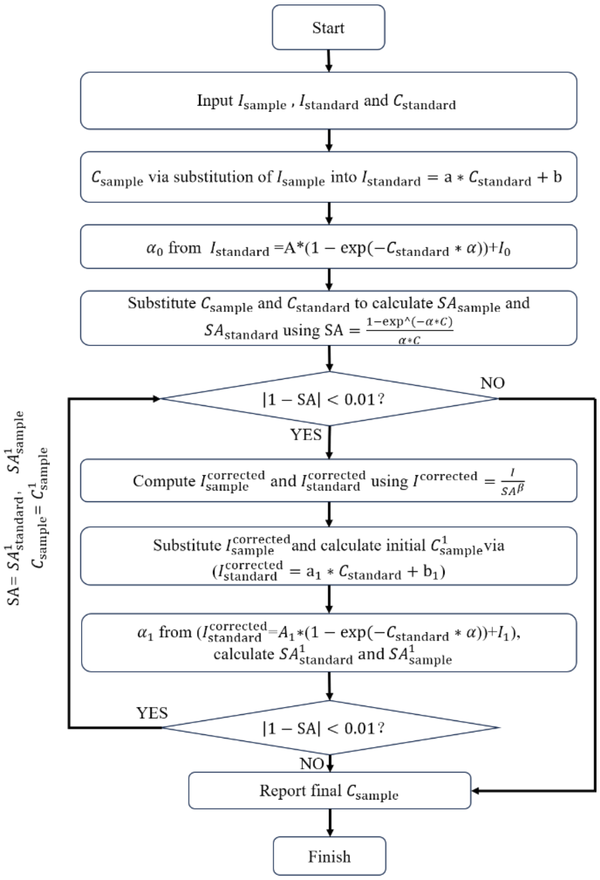

Fig. 2 Flowchart of the self-absorption correction method based on SA iteration.

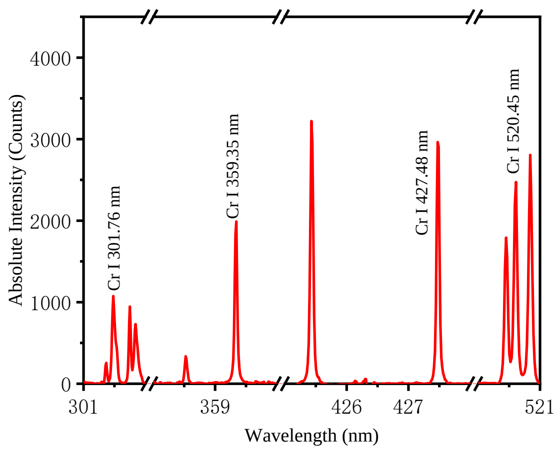

Fig. 3 SENLIBS spectrum of standard sample with 5 ppm Cr.

Methodology. The self-absorption was evaluated by fitted the calibration curve of concentration and spectral intensity with the exponential function, which can be expressed as[19]:

$$I(c) = \mathrm{A}(1 - e^{-\alpha c}) + I_0 \tag{1}$$

where c and $I(c)$ represent the elemental concentration and spectral line intensity. I_0 and α are the intensity arising from systematic error. and self-absorption parameter, which are obtained by fitting parameters of calibrate curve. Then the SA can be calculated as:

$$SA = \frac{1 - e^{-\alpha c}}{\alpha c} \tag{2}$$

As the SA also can be calculated with the non-self-absorbed intensity $I_r(c)$, which can be expressed as [26, 33]:

$$SA^{\beta} = \frac{I(c)}{I_r(c)} \tag{3}$$

where β is 0.46. And the spectral intensity after SA calibration is expressed as:

$$I_r(c) = \frac{I(c)}{SA^{\beta}} \tag{4}$$

According to Equation (3), a unit value of SA indicates the absence of self-absorption. This principle forms the basis of the iterative correction algorithm developed in this work, which aims to progressively refine the spectral intensity until $|1 - SA| < 0.01$. The detailed procedure illustrated in the flowchart of Fig. 2, which is outlined below:

(1) Initial measurement: measure the spectral line intensities for the unknown sample (I_{sample}) and a set of standard samples with known concentrations C_{std} ($I_{standard}$) (see Step 1 in Fig. 2).

(2) Preliminary linear calibration: perform an ordinary least squares regression with an intercept on the standard samples to establish an initial calibration model: $I_{standard} = a * C_{standard} + b$. estimate the initial concentration of the unknown sampleC_{sample}, by inserting I_{sample} into this model (see Step 2 in Fig. 2).

(3) Nonlinear fitting for self-absorption parameter: fit the standard sample data ($I_{standard}$ and $C_{standard}$) using the nonlinear model in equation (1) to determine the initial self-absorption parameter α_0 (see Step 3 in Fig. 2).

(4) Calculate initial SA: substitute C_{sample} and $C_{standard}$ into equation (2) to compute the initial SAs for the unknown sample (SA_{sample}) and standard sample ($SA_{standard}$) (see Step 4 in Fig. 2).

(5) Convergence check: if both SA_{sample} and $SA_{standard}$are sufficiently close to 1 (e.g., SA > 0.99), self-absorption is deemed negligible, and C_{sample} is accepted as the final concentration (see Step 5 in Fig. 2).

(6) Intensity correction: if SA values are significantly below 1, correct the intensities I_{sample} and $I_{standard}$ using equation (4), obtaining $I^{corrected}_{sample}$ and $I^{corrected}_{standard}$ (see Step 6 in Fig. 2).

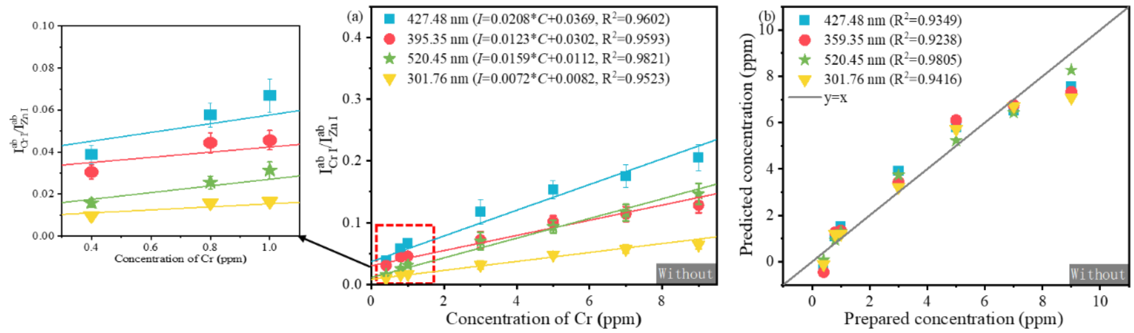

Fig. 4 Quantitative analysis of Cr I without self-absorption correction: (a) calibration curve and (b) correlation curve of predicted vs. prepared concentrations.

(7) Refined linear calibration: establish a new linear calibration model using the corrected standard data ($I_{standard}^{corrected}$ and $C_{standard}$). estimate an updated concentration for the unknown sample C_{sample}^{1}, using $I_{sample}^{corrected}$ (see Step 7 in Fig. 2).

(8) Parameter update and re-evaluation: refit equation (1) using the corrected standard data ($I_{standard}^{corrected}$ and $C_{standard}$) to update the self-absorption parameter to α_1. Recalculate the SA values (SA_{sample}^{1} *and* $SA_{standard}^{1}$) using the updated concentration C_{sample}^{1} and the new parameter α_1. If the new SA values are close to 1, output C_{sample}^{1} as the result (see Step 8 in Fig. 2).

(9) Iteration: if self-absorption remains significant (SA < 0.99), update the variables with the new values (e.g., set $SA = SA_1$ and C_{sample}= C_{sample}^{1}) and repeat steps 5 through 8. The iteration continues until the SA values converge to approximately 1, yielding the final corrected concentration (see Step 9 in Fig. 2 and cyclic arrow).

Qualitative analysis. The typical SENLIBS spectrum of standard sample with 5 ppm Cr is shown in Fig. 3. As shown in the wavelength range of 301-521 nm, the neutral Cr lines are found. The detailed list of spectral parameters for Cr I lines, derived from the NIST database, is presented in Table S2. The SA values were calculated using equations (1) and (2) with the concentration of 5 ppm. To verify the universality of self-absorption correction method based on SA iteration, four lines with SA values from 0.496 to 0.740 were selected for calibration curves, which are marked in the Fig. 3 and Table S2. The Cr I 427.48 nm and Cr I 359.35 nm are resonance lines, which exhibits a strong self-absorption effect. The Cr I 520.45 nm and Cr I 301.76 nm, which transition from non-ground states and exhibit weaker self-absorption effects.

RESULTS AND DISCUSSION

Quantitative analysis without self-absorption correction. To evaluate the impact of the self-absorption effect on quantitative analysis, calibration curves of concentration versus spectral intensity were established for the four selected Cr I lines (427.48 nm, 359.35 nm, 520.45 nm, and 301.76 nm), followed by linear fitting. To mitigate spectral fluctuations during the experiment, the Zn I 468.01 nm line from the substrate was used as an internal reference for intensity normalization. Fig. 4 shows the calibration curves and correlation curve of predicted vs. prepared concentrations for the Cr I 427.48 nm, Cr I 359.35 nm, Cr I 520.45 nm, and Cr I 301.76 nm lines. As shown in Fig. 4(a), the calibration curves for the four lines exhibit a certain degree of linearity, with the coefficient of determination (R^2) values of 0.9602, 0.9593, 0.9821, and 0.9532, and slopes of 0.0208, 0.0123, 0.0159, and 0.0072 ppm^{-1}, respectively. Furthermore, the nonlinear model (Equation (1)) was used to calculate the α values for the four lines, which were 0.5567, 0.6818, 0.2958, and 0.4306, respectively. Based on Equation (2), the ranges of the SA for the four lines were determined to be 0.2000–0.8964, 0.1626–0.8752, 0.3494–0.9431, and 0.2527–0.9186, respectively. These results indicate the presence of self-absorption effects in the calibration curves of the four lines. The predicted concentrations were further calculated using the leave-one-out cross-validation (LOOCV) method, as shown in Fig. 4(b), the R^2 between the predicted and prepared concentrations are 0.9349, 0.9238, 0.9805, and 0.9416, respectively. As summarized in Table 1, before self-absorption correction, the average relative errors (ARE) between the predicted and prepared concentrations for the Cr I 427.48 nm, Cr I 359.35 nm, Cr I 520.45 nm, and Cr I 301.76 nm lines were 48.40%, 51.82%, 24.88%, and 34.66%, respectively; the root mean square errors of cross-validation (RMSECV) were 0.820, 0.872, 0.489, and 0.827 ppm, respectively; and the limits of detection (LOD) were 0.053, 0.048, 0.018, and 0.354 ppm, respectively. It is evident that the self-absorption effect significantly compromises the accuracy of the calibration curves, necessitating further correction.

Quantitative analysis with iterative self-absorption correction. To correct the self-absorption effect, present in the calibration curves, an iterative method based on the SA was applied in this study. Fig. 5 illustrates the influence of the number of iterations on the SA and the relative error (RE) of prediction at low, medium, and high concentrations. As shown in Fig. 5(a), higher concentrations result in lower SA values, indicating more severe

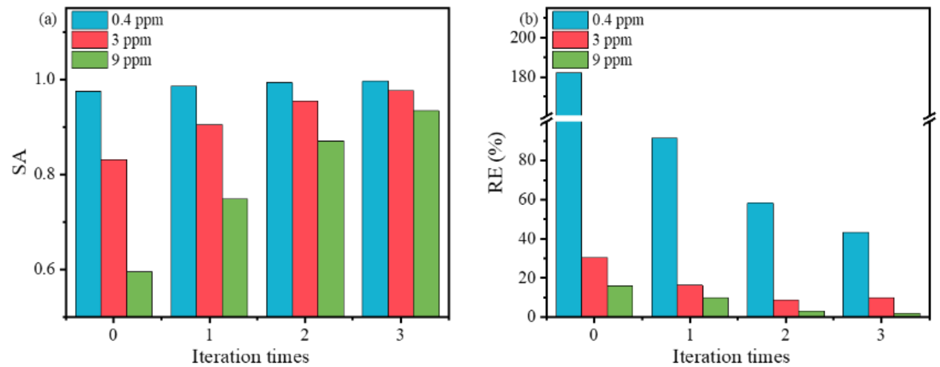

Fig. 5 Relationship between the number of iterations and the SA and RE values.

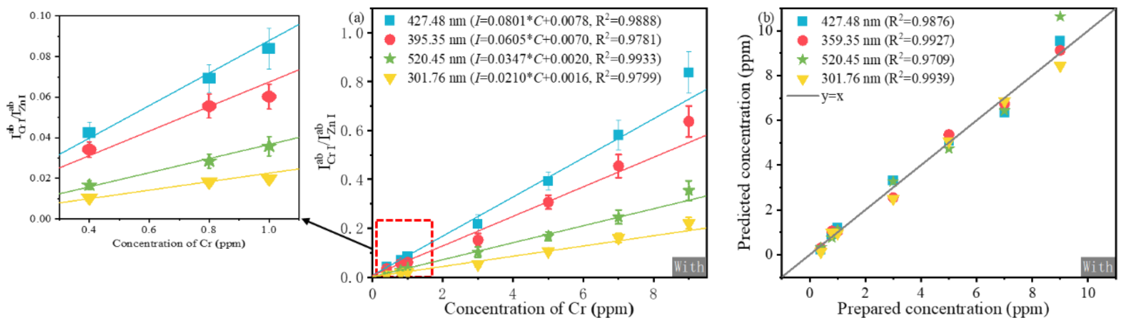

Fig. 6 Quantitative analysis of Cr I with self-absorption correction: (a) calibration curve and (b) correlation curve of predicted vs. prepared concentrations.

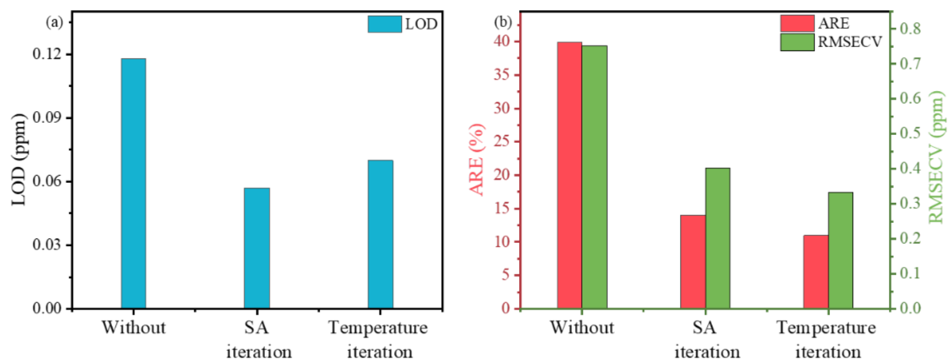

Fig. 7 (a) LOD and (b) ARE and RMSECV values: without the self-absorption correction, with the SA-based method, and with the temperature iteration method.

self-absorption. With an increasing number of iterations, the SA values for 0.4, 3, and 9 ppm gradually increase and approach 1. Correspondingly, as depicted in Fig. 5(b), the relative error of the predicted concentrations decreases progressively with the number of iterations. These results demonstrate that the proposed iterative self-absorption correction method can progressively mitigate prediction errors caused by self-absorption, thereby improving the accuracy of quantitative analysis.

Figure 6 further displays the calibration curves and correlation curve of predicted vs. prepared concentrations for the Cr I 427.48 nm, Cr I 359.35 nm, Cr I 520.45 nm, and Cr I 301.76 nm lines with self-absorption correction. As shown in Fig. 6(a), the R^2 of the calibration curves were improved to 0.9888, 0.9781, 0.9933, and 0.9799, respectively, and the slopes increase to 0.0801, 0.0605, 0.0347, and 0.0210 ppm^{-1}, indicating enhanced linearity and sensitivity. Moreover, the SA values of the spectral lines calculated using Equations (1) and (2) are all greater than 0.99, further confirming the effective correction of the self-absorption effect. As shown in Fig. 6(b), the R^2 between the predicted and prepared concentrations have improved to 0.9876, 0.9927, 0.9709, and 0.9939, respectively. As summarized in Table 1 and Fig. 7, after self-absorption correction, the ARE between the predicted and prepared concentrations for the four Cr I lines are reduced to 14.59%,

Table 1. LOD, ARE, and RMSECV without and with the SA iteration method

λ (nm)	ARE (%)		RMSECV (ppm)		LOD (ppm)	
	Without	With	Without	With	Without	With
427.48	48.40	14.59	0.820	0.355	0.053	0.014
359.35	51.82	12.63	0.872	0.268	0.048	0.010
520.45	24.88	11.08	0.489	0.673	0.018	0.081
301.76	34.66	17.69	0.827	0.317	0.354	0.122
Average	39.94	14.00	0.752	0.403	0.118	0.057

Table 2. LOD, ARE, and RMSECV with the temperature iteration method

λ (nm)	ARE (%)	RMSECV (ppm)	LOD (ppm)
427.48	17.20	0.302	0.034
359.35	7.73	0.424	0.020
520.45	10.58	0.382	0.013
301.76	8.54	0.222	0.213
Average	11.01	0.333	0.070

12.63%, 11.08%, and 17.69%, respectively; the RMSECV values are 0.355, 0.268, 0.673, and 0.317 ppm, respectively; and the LODs are lowered to 0.014, 0.010, 0.081, and 0.122 ppm, respectively. Overall, the average ARE decreases from 39.94% to 14.00%, the average RMSECV reduced from 0.752 ppm to 0.403 ppm, and the average LOD improves from 0.118 ppm to 0.057 ppm. These results indicate that the iterative SA method proposed in this study effectively enhances the quantitative accuracy of the calibration curves.

Performance comparison of correction methods. Temperature iteration-based self-absorption correction is a method for reducing the self-absorption effect that relies on the plasma thermal equilibrium radiation model[26]. It continuously calculates and corrects the plasma electron temperature and the product of radiating particle number density and absorption path length, without depending on the Stark broadening coefficient, to improve the linearity and accuracy of LIBS quantitative analysis and obtain reliable plasma parameters. In this study, the spectral lines of Cr I 427.48, 359.35, 520.84, 520.60, 520.45, 540.98, 435.17, 301.76, and 434.45 nm were used to calculate the plasma temperature. Table 2 presents the LOD, ARE and RMSECV for Cr obtained via temperature iteration method. As shown, the temperature iteration method reduced the average ARE of Cr I 427.48 nm, Cr I 359.35 nm, Cr I 520.45 nm, and Cr I 301.76 nm to 11.01%, the average RMSECV to 0.333 ppm, and the average LOD to 0.070 ppm. In contrast, the proposed SA iteration method for self-absorption correction achieved an average relative error of 14.00%, indicating that the two methods possess comparable quantitative accuracy. Furthermore, the proposed method achieved a lower average LOD of only 0.057 ppm.

However, the most significant advantage of the proposed method lies in its markedly reduced operational complexity. The temperature iteration method, while highly accurate, requires the construction of a Boltzmann plot and iterative calculation of plasma temperature, which necessitates a set of well-characterized spectral lines and introduces considerable computational complexity. In contrast, our method operates solely on the intensity-concentration relationship of the analytical line itself, completely bypassing the need for complex plasma diagnostics. This makes the SA coefficient iteration an efficient and practical alternative, achieving competitive analytical performance with greatly simplified implementation for routine analysis.

CONCLUSION

The SA iteration method is proposed and validated as an effective approach for mitigating the self-absorption effect in SENLIBS. This method iteratively refines spectral intensities using an SA parameter directly derived from the calibration curve, progressively converging SA values toward unity. When applied to the quantitative analysis of trace Cr in aqueous samples, the method markedly enhanced the linearity of calibration curves, with all post-correction R^2 values surpassing 0.97. A head-to-head comparison with the temperature iteration method using the same dataset confirms that the proposed SA iteration method exhibits highly competitive analytical performance: its ARE was 14.00%, comparable to that of the temperature iteration method, while its average LOD was lower at 0.057 ppm. The most notable advantage of this method lies in its drastically simplified operational workflow, as it eliminates the need for complex plasma temperature calculations and the requirement for multiple spectral lines. This achieves an excellent balance between analytical accuracy and operational simplicity. Collectively, these results validate the SA iteration method as a robust, efficient, and practical correction technique that enhances the quantitative accuracy of SENLIBS without introducing additional experimental or computational complexity. While the method has demonstrated efficacy within the validated system, its general applicability to other elements, matrices, or experimental configurations (*e.g.*, different substrates or laser systems) requires further investigation. Future work will focus on extending the validation to other elements and matrices, as well as exploring the potential integration of this iterative framework with other calibration strategies to further enhance the robustness and scope of LIBS quantitative analysis.

ASSOCIATED CONTENT

The supporting information (Tables S1-S2) is available at https://www.at-spectrosc.com.

AUTHOR INFORMATION

Xinyan Yang received her Ph.D. from Huazhong University of Science and Technology in 2017. She currently serves as an Associate Professor and Master's Supervisor at the School of Physics and Electronic Information, Anhui Normal University. Research Interests: Development of performance improvement methods and theoretical research on Laser-Induced Breakdown Spectroscopy (LIBS) quantitative analysis.

Corresponding authors

* X. Y. Yang

E-mail address: xinyanyang@ahnu.edu.cn

Notes

The authors declare no competing financial interest.

ACKNOWLEDGMENTS

This work received financial support from the National Natural Science Foundation of China (61805002 and 12474255), Anhui Provincial Key Research and Development Program (1804a0802193) and Anhui Provincial Natural Science Foundation (2208085Y02).

REFERENCES

1. M. A. Aguirre, S. Legnaioli, F. Almodóvar, M. Hidalgo, V. Palleschi, and A. Canals, *Spectrochim. Acta B*, 2013, **79–80**, 88-93. https://doi.org/10.1016/j.sab.2012.11.011
2. Y. T. Wang, H. L. Li, X. L. Yin, C. X. Zhang, X. T. Li, and L. D. Fang, *Measurement*, 2024, **224**, 113869. https://doi.org/10.1016/j.measurement.2023.113869
3. Q. Y. Wang, T. Ge, Y. T. Liu, L. Y. Jiang, A. M. Chen, J. H. Han, and M. X. Jin, *J. Anal. At. Spectrom.*, 2022, **37**, 233-239. https://doi.org/10.1039/d1ja00415h
4. X. Y. Yang, Z. Q. Hao, M. Shen, R. X. Yi, J. M. Li, H. W. Yu, L. B. Guo, X. Y. Li, X. Y. Zeng, and Y. F. Lu, *Talanta*, 2017, **163**,127-131. https://doi.org/10.1016/j.talanta.2016.10.094
5. J. M. Li, L. B. Guo, C. M. Li, N. Zhao, X. Y. Yang, Z. Q. Hao, X. Y. Li, X. Y. Zeng, and Y. F. Lu, *Opt. Lett.*, 2015, **40**, 5224-5226. https://doi.org/10.1364/OL.40.005224
6. W. Skrzeczanowski and M. Dlugaszek, *Materials*, 2022, **15**, 3736. https://doi.org/10.3390/ma15103736
7. N. Schlatter, B. G. Lottermoser, S. Illgner, and S. Schmidt, *Chemosensors*, 2023, **11**, 479. https://doi.org/10.3390/chemosensors11090479
8. J. J. Hou, L. Zhang, Y. Zhao, Z. Wang, Y. Zhang, W. G. Ma, L. Dong, W. B. Yin, L. T. Xiao, and S. T. Jia, *Plasma Sci. Technol.*, 2019, **21**, 034016. https://doi.org/10.1088/2058-6272/aaf875
9. F. Rezaei, G. Cristoforetti, E. Tognoni, S. Legnaioli, V. Palleschi, and A. Safi, *Spectroc. Acta B*, 2020, **169**, 105878. https://doi.org/10.1016/j.sab.2020.105878
10. Evgueni, Gudimenko, Vladimir, Milosavljevic, Stephen, and Daniels, *Opt. Express*, 2012, **20**, 12699-12709. https://doi.org/10.1364/OE.20.012699
11. R. X. Yi, L. B. Guo, C. M. Li, X. Y. Yang, J. M. Li, X. Y. Li, X. Y. Zeng, and Y. F. Lu, *J. Anal. At. Spectrom.*, 2016, **31**, 961-967. https://doi.org/10.1039/c5ja00500k
12. T. Fei, C. Y. Pan, Q. Zeng, Q. P. Wang, and X. W. Du, *Plasma Sci. Technol.*, 2018, **20**, 045503. https://doi.org/10.1088/2058-6272/aaaada
13. J. A. Aguilera, J. Bengoechea, and C. Aragón, *Spectrochim. Acta B*, 2003, **58**, 221-237. https://doi.org/10.1016/S0584-8547(02)00258-6
14. Y. Tang, S. Ma, Y. Chu, T. Wu, Y. Ma, Z. Hu, L. Guo, X. Zeng, J. Duan, and Y. Lu, *Opt. Express*, 2019, **27**, 4261-4270. https://doi.org/4270. 10.1364/OE.27.004261
15. C. Y. Diao, C. S. Chen, B. Y. Man, C. Wang, and H. B. Fu, *Eur. Phys. J. D*, 2011, **63**, 123-128. https://doi.org/10.1140/epjd/e2011-10394-y
16. H. B. Fu, C. S. Chen, B. Y. Man, X. Song, and D. Liu, *Eur. Phys. J. D*, 2011, **65**, 509-513. https://doi.org/10.1140/epjd/e2011-20265-2
17. I. Karnadi, M. Pardede, I. Tanra, R. Hedwig, A. M. Marpaung, Z. S. Lie, E. Jobiliong, D. Kwaria, M. M. Suliyanti, M. Ramli, K. Lahna, T. J. Lie, H. Suyanto, K. H. Kurniawan, and K. Kagawa, *Sci. Rep.*, 2020, **10**, 13278. https://doi.org/10.1038/s41598-020-70151-6
18. M., Burger, M., Skocic, S., and Bukvic, *Spectrochim. Acta B*, 2014, **101**, 51-56.
19. J. M. Li, Y. Tang, Z. Q. Hao, N. Zhao, X. Y. Yang, H. W. Yu, L. B. Guo, X. Y. Li, X. Y. Zeng, and Y. F. Lu, *J. Anal. At. Spectrom.*, 2017, **32**, 2189-2193. https://doi.org/10.1039/c7ja00199a
20. Y. Tang, X. X. Peng, Z. L. Hu, J. F. Li, Z. Q. Hao, X. Y. Yang, S. X. Ma, R. Yuan, and L. B. Guo, *J. Anal. At. Spectrom.*, 2022, **37**, 1535-1540. https://doi.org/10.1039/d2ja00100d
21. I. B. Gornushkin, J. M. Anzano, L. A. King, B. W. Smith, N. Omenetto, and J. D. Winefordner, *Spectrochim. Acta B*, 1999, **54**, 491-503. https://doi.org/10.1016/S0584-8547(99)00004-X

22. D. Bulajic, M. Corsi, G. Cristoforetti, S. Legnaioli, V. Palleschi, A. Salvetti, and E. Tognoni, *Spectrochim. Acta B*, 2002, **57**. 339-353. https://doi.org/10.1016/S0584-8547(01)00398-6
23. S. A. M. Mansour, *Opt. Photonics J.*, 2015, **5**, 79-90. https://doi.org/10.4236/opj.2015.53007
24. L. Sun and H. Yu, *Talanta*, 2009, **79**, 388-395. https://doi.org/10.1016/j.talanta.2009.03.066
25. C. Aragón, J. Bengoechea, and J. A. Aguilera, *Spectrochim. Acta B*, 2001, **56**, 619-628. https://doi.org/10.1016/S0584-8547(01)00172-0
26. J. J. Hou, D. C. Zhang, Z. Q. Feng, J. F. Zhu, and L. Zhang, *Spectrochim. Acta B*, 2024, **215**, 106925. https://doi.org/10.1016/j.sab.2024.106925
27. Y. Q. Zhang, Y. Lu, Y. Tian, Y. Li, W. Q. Ye, J. J. Guo, and R. E. Zheng, *Anal. Chim. Acta*, 2022, **1195**, 339423. https://doi.org/10.1016/j.aca.2021.339423
28. T. Li, Z. Hou, Y. Fu, J. Yu, W. Gu, and Z. Wang, *Anal. Chim. Acta*, 2019, **1058**, 39-47. https://doi.org/10.1016/j.aca.2019.01.016
29. F. Rezaei, P. Karimi, and S. H. Tavassoli, *Appl. Phys B-Lasers O.*, 2014, **114**, 591-600. https://doi.org/10.1007/s00340-013-5566-3
30. J. Dong, L. Liang, J. Wei, H. S. Tang, T. L. Zhang, X. F. Yang, K. Wang, and H. Li, *J. Anal. At. Spectrom.*, 2015, **30**, 1336-1344. https://doi.org/10.1039/c4ja00470a
31. J. H. Yang, X. M. Li, J. W. Xu, and X. H. Ma, *Appl. Spectrosc.*, 2018, **72**, 129-140. https://doi.org/10.1177/0003702817734293
32. X. Y. Yang, D. D. Li, Z. Z. Zhang, X. Zhang, P. Zhu, C. Liu, T. Hong, H. M. Ren, Z. F. Hua, Z. F. Sun, Z. B. Qin, and X. F. Zheng, *Anal. Methods*, 2024, **16**, 8278-8283. https://doi.org/10.1039/d4ay01718h
33. A. M. El Sherbini, T. M. El Sherbini, H. Hegazy, G. Cristoforetti, S. Legnaioli, V. Palleschi, L. Pardini, A. Salvetti, and E. Tognoni, *Spectrochim. Acta B*, 2005, **60**, 1573-1579. https://doi.org/10.1016/j.sab.2005.10.011